The division of amyloid fibrils – Systematic comparison of fibril fragmentation stability by linking theory with experiments

BEAL, David M <http://orcid.org/0000-0002-1819-315X>, TOURNUS, Magali, MARCHANTE, Ricardo <http://orcid.org/0000-0003-3153-6329>, PURTON, Tracey, SMITH, David <http://orcid.org/0000-0001-5177-8574>, TUITE, Mick F <http://orcid.org/0000-0002-5214-540X>, DOUMIC, Marie and XUE, Wei-Feng <http://orcid.org/0000-0002-6504-0404>

The division of amyloid fibrils – Systematic comparison of fibril fragmentation stability by linking theory with experiments

David M. Beal, Magali Tournus, Ricardo Marchante, Tracey Purton, David P. Smith, Mick F. Tuite, Marie Doumic, Wei-Feng Xue

PII: S2589-0042(20)30704-5

DOI: https://doi.org/10.1016/j.isci.2020.101512

Reference: ISCI 101512

To appear in: *ISCIENCE*

Received Date: 16 March 2020

Revised Date: 31 July 2020

Accepted Date: 26 August 2020

Please cite this article as: Beal, D.M., Tournus, M., Marchante, R., Purton, T., Smith, D.P., Tuite, M.F., Doumic, M., Xue, W.-F., The division of amyloid fibrils – Systematic comparison of fibril fragmentation stability by linking theory with experiments *ISCIENCE* (2020), doi: https://doi.org/10.1016/j.isci.2020.101512.

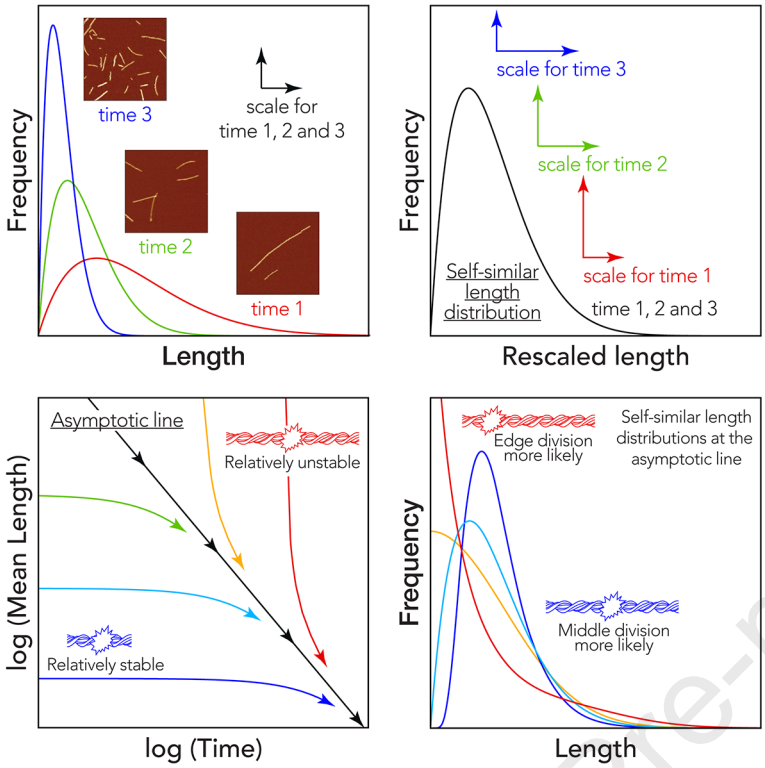

The division of amyloid fibrils – Systematic comparison of fibril fragmentation stability by linking theory with experiments

David M. Beal[1], *Magali Tournus*[2], *Ricardo Marchante*[1,6], *Tracey Purton*[1], *David P. Smith*[3], *Mick F. Tuite*[1], *Marie Doumic*[4,5], *Wei-Feng Xue*[1,4,†,‡]

[1]Kent Fungal Group, School of Biosciences, University of Kent, CT2 7NJ, Canterbury, UK, [2]Centrale Marseille, I2M, UMR 7373, CNRS, Aix-Marseille univ., Marseille, 13453, France [3]Biomolecular Research Centre, Sheffield Hallam University, Sheffield, UK [4]INRIA Rocquencourt, équipe-projet BANG, domaine de Voluceau, BP 105, 78153 Rocquencourt, France [5]Wolfgang Pauli Institute, University of Vienna, Vienna, Austria [6]Current address: Institute for Genetics and CECAD Research Center, University of Cologne, Joseph-Stelzmann Str. 26, 50931 Cologne, Germany

[†]Lead contact

[‡]Correspondence to: W.F.Xue@kent.ac.uk; Tel +44-(0)1227 824821

SUMMARY

The division of amyloid protein fibrils is required for the propagation of the amyloid state, and is an important contributor to their stability, pathogenicity and normal function. Here, we combine kinetic nanoscale imaging experiments with analysis of a mathematical model to resolve and compare the division stability of amyloid fibrils. Our theoretical results show that the division of any type of filament results in self-similar length distributions distinct to each fibril type and the conditions applied. By applying these theoretical results to profile the dynamical stability towards breakage for four different amyloid types, we reveal particular differences in the division properties of disease-related amyloid formed from alpha-synuclein when compared with non-disease associated model amyloid, the former showing lowered intrinsic stability towards breakage and increased likelihood of shedding smaller particles. Our results enable the comparison of protein filaments' intrinsic dynamic stabilities, which are key to unravelling their toxic and infectious potentials.

INTRODUCTION

Amyloid fibrils, proteinaceous polymers with a cross-beta core structure, represent an important class of bio-nanomaterials (Bleem and Daggett, 2017; Knowles and Buehler, 2011). They are also important biological structures associated with devastating human diseases such as Alzheimer's disease, Parkinson's disease, Creutzfeldt-Jakob disease (CJD), systemic amyloidosis and type 2 diabetes (Knowles et al., 2014), as well as having vital biological functions such as adhesion and biofilm formation, epigenetic switches, and hormone storage (e.g. Berson et al., 2003; Bleem and Daggett, 2017; Chapman et al., 2002; Knowles and Buehler, 2011; Larsen et al., 2007; Li et al., 2014; Romero et al., 2010; Tuite and Serio, 2010). Division of amyloid fibrils, which can manifest *in vitro* in amyloid nanomaterials or *in vivo* in disease-associated or functional amyloid aggregates, is mediated by mechanical agitation, thermal stress, chemical perturbation or chaperone catalysis. Fibril division is a crucial step in the life-cycle of amyloid (**Fig. 1a**) (Xue, 2015) and enables the propagation of the amyloid protein conformation and biological information encoded therein. Despite knowledge of its importance, it is not understood why amyloid division processes give rise to varied biological impacts ranging from normal propagation of functional amyloid assemblies to large inert structures or the creation of molecular species involved in disease, e.g. small cytotoxic amyloid species and infective prions, which are transmissible amyloid particles. In this respect, the resistance of amyloid to division is also a critical aspect to protein misfolding associated with disease progression and biological roles of functional amyloid assemblies (e.g. Tanaka et al., 2006). In terms of disease association, there is much debate as to how amyloid aggregates are associated with cellular toxicity, with evidence of both prefibrillar oligomers and fibrillar species (Breydo and Uversky, 2015; Tipping et al., 2015) giving rise to disease-related phenotypes. While it is hypothesised that all proteins can undergo conversion into an amyloid state (Dobson, 1999), why most proteins do not form amyloid under physiological conditions or produce amyloid particles that are non-toxic, non-

transmissible or non-disease associated is not clear. In this debate, it has been suggested that fibrils are not merely the end product of amyloid aggregation, but rather elicit profound biological responses through fibril fragmentation and oligomer shedding (Tipping et al., 2015), due to lack of fibril stability.

Amyloid fibrils have remarkable physical properties, such as their tensile strength comparable to that of steel and elasticity similar to spider silk (Knowles et al., 2007). As proteinaceous polymers, they also offer the potential for modification by rational design, which makes them an ideal target for the development of biologically compatible nanomaterials (Bleem and Daggett, 2017; Hu et al., 2018; Li et al., 2014; Mankar et al., 2011). This interest in amyloid as a bio-nanomaterial has led to a search for proteins and peptides which can undergo conversion into a stable amyloid conformation while lacking the properties that associate them with toxicity, infectivity and disease. Though the precise properties that associate some amyloid to disease or biological function are not resolved, the potential for different morphologies (sometimes referred to as 'strains') to elicit different results (Meinhardt et al., 2009; Sachse et al., 2010; Tanaka et al., 2006) could be attributed to the stability of amyloid fibrils towards division or their mechanical properties (Marchante et al., 2017; Xue et al., 2009a). Thus, the stability of amyloid fibrils is an important physical factor which modulates their biological function of amyloid and potential as a nanomaterial.

The kinetics of the nucleated growth of amyloid fibrils are profoundly influenced by secondary processes such as fibril fragmentation/breakage (Knowles et al., 2009; Xue et al., 2008) and secondary surface nucleation (Buell et al., 2014; Tornquist et al., 2018) (**Fig. 1a**). These processes determine the rate of the exponential growth phase of amyloid assembly alongside with growth by elongation at fibril ends (Lorenzen et al., 2012; Xue et al., 2008). As one of the key secondary processes, fibril fragmentation stands out compared to the other three main processes (**Fig. 1a**) in that it reduces aggregate size at the same time as it increases the number of aggregates (Xue et al., 2009a).

In this aspect, fibril fragmentation results in the division of amyloid fibrils analogous to a microbial or cellular division process. Resistance to fibril fragmentation is linked to the mechanical stability of amyloid fibrils, which has implications for both the development of nanomaterials and on the understanding of amyloid disease-associated biological processes. The mechanism and the rate of fibril fragmentation have been subjected to theoretical considerations (Hill, 1983; Knowles et al., 2009; Paparcone and Buehler, 2011; Xue et al., 2008) and experimental investigations involving fragmentation promoted by mechanical perturbations (Nicoud et al., 2015; Xue et al., 2008; Xue and Radford, 2013). The fragmentation of protein filaments is a length dependent process whereby longer particles break more easily than short ones. This length-dependent breakage of amyloid fibrils can follow a strong, non-linear dependence where longer fibrils are progressively less stable towards breakage per monomeric unit relative to their shorter counterparts (Xue and Radford, 2013). Thus, the fibrils' resistance to division, and in turn the inherent stability of the fibrils, is an important and measurable property (Xue and Radford, 2013) that will help rationalise phenomena such as prion strains, polymorphism, transmission, amyloid toxicity, biofilm formation and epigenetic regulation (e.g. Aguzzi et al., 2007; Cox et al., 2003; Derdowski et al., 2010; Lee et al., 2011; Lin et al., 2017; Marchante et al., 2017; Shorter and Lindquist, 2004; Sondheimer and Lindquist, 2000; Tanaka et al., 2006; Xue et al., 2009a; Zeng et al., 2015) and lead to a better understanding of amyloid-associated diseases.

The division of amyloid polymers into small more infective particles, either through environmental perturbations or through catalysis by molecular chaperones, is key to the spreading of prion phenotypes (Cox et al., 2003; Marchante et al., 2017). For example, the propagation of the yeast prion phenotype [PSI^{+}] associated with yeast Sup35 protein assemblies relies on the fragmentation activity of the chaperon Hsp104 and its co-chaperones (Chernoff et al., 1995; Shorter and Lindquist, 2004). The resistance of Sup35 assemblies to fragmentation correlates with the formation of different [PSI^{+}] phenotypes (Tanaka et al., 2006). In addition, the smaller particles generated by fibril fragmentation show enhanced cytotoxicity when compared with the larger parent fibrils (Xue et al., 2009a), likely

due to a higher propensity to interact with cell membranes, entering cells by endocytosis, interacting with the lysosome and inducing cytotoxicity by disrupting proteostasis (Ankarcrona et al., 2016; Hu et al., 2009; Jakhria et al., 2014; Marchante et al., 2017; Milanesi et al., 2012). The stability of amyloid fibrils towards division is, therefore, an important characteristic of amyloid fibrils that must be considered if we are to understand the biological activity and nanomaterial properties of amyloid. Because protein filaments formed from different precursors show a variety of suprastructures and size distributions (e.g. Barritt et al., 2017; Knowles et al., 2007; Meinhardt et al., 2009; Xue et al., 2009a), no unifying theory has been developed for the division of amyloid fibrils. As consequence, the stability towards division for different types of amyloid fibrils with varied suprastructures that ranges from inert network of long filaments to infectious particles is yet to be systematically measured, determined and compared.

We have previously shown that the time evolution of amyloid fibril length distributions obtained by nanoscale atomic force microscopy (AFM) imaging contain valuable information on the rate, length-dependence and position-dependence of fibril fragmentation that can be extracted (Xue and Radford, 2013). However, since fibril division is itself a strongly length-dependent process, systematic comparison of the stability of fibrils towards division and their division rates has been hampered by the varied length distributions of different types of amyloid fibrils. Currently, the links between data and theory that would allow direct comparison of the fibrils' division propensities are also missing. Here, we have developed an analytical approach that enables direct determination of the dynamic stability of amyloid fibrils towards division from fibril length distributions. We have developed a new theory on amyloid fibril division that shows how the division mechanism of amyloid fibrils and their stability towards division dictates the exact shape of the resulting length distributions. We then established an analytical method to extract a set of unique and intrinsic properties of the fibril stability to division from image data of pre-formed fibrils undergoing physical fragmentation experimentally promoted by mechanical perturbation. Demonstrating the utility of our combined experimental and theoretical approach, we determined and compared the division of fibril samples formed from human

α-synuclein (α-Syn) associated with Parkinson's disease with fibrils formed from β-lactoglobulin (β-Lac) and lysozyme (Lyz). We have also reanalysed and compared previously published fibril fragmentation data of β_2-microglobulin (β_2m) under the same mechanical perturbation regime (Xue and Radford, 2013). Comparison of the dynamic stability of these fibrils types of different origin revealed different division properties, with fibrils formed from the human Parkinson's disease-associated α-Syn being the least overall stable and prone to generate small sub 100 nm particles that may possess enhanced cytotoxic and prion-like infectious potential (Brundin and Melki, 2017). The ability to assess and compare the division properties of amyloid fibrils, enumerated as parameters extractable from experimental data, enables the prediction of an amyloid's propensity to generate toxic and infectious particles, and therefore has a significant impact on the understanding of their roles in biology, in diseases, and their application as a functional bio-nanomaterial.

RESULTS

Amyloid fibrils of diverse suprastructures and length distributions fragment to different extents upon mechanical perturbation

To demonstrate that the fibril division rates, indicative of their dynamic stability to division, can be assessed and compared for amyloid fibrils with diverse suprastructures and length distributions, we first collected experimental AFM image data sets of amyloid fibrils, pre-formed from different precursors, undergoing division through fragmentation promoted by mechanical stirring. These experiments were designed to isolate the fibril division processes from other growth processes and to generate data that contain sufficient quality and quantity of information on the division of fibril particles under identical mechanical perturbation regimes to enable comparison. Here, we chose to

investigate the human disease-associated amyloid system α-Syn alongside bovine β-Lac and chicken egg white Lyz as biophysical model systems not directly related to human disease. Samples were formed containing long, straight fibrils from these three proteins *in vitro*, and validated by negative-stain Electron Microscopy imaging (**Supplementary Fig. S1**). Lyz and β-Lac were both converted to their fibrillar amyloid form by heating under acidic conditions (pH 2.0), commonly used conditions for the assembly of these proteins *in vitro*. α-Syn fibrils were prepared from freshly purified recombinant α-Syn monomers (Cappai et al., 2005) at 37^{o}C under physiological pH. For each fibril sample, 500 µl of 120 µM monomer equivalent fibril solutions in their respective fibril forming buffer were then stirred at 1000 rpm by a 3 x 8mm magnetic stirrer bar in a 1.5ml glass chromatography vial using the same mechanical perturbation method as previously reported (Xue and Radford, 2013) using an Ika Squid stirrer plate with a digital display. The *in vitro*-formed fibril samples were initially dispersed by 5-10 min of stirring and were subsequently deposited onto freshly cleaved mica surfaces and imaged by AFM (**Fig. 2** left most column).

As seen in the leftmost column of images in **Fig 2.**, the initial samples after brief stirring to disperse the fibril particles show long, straight, elongated, unbranched nano-structures expected for amyloid fibrils. However, whereas Lyz and α-Syn form fibrils that exhibit more flexibility and curvature, β-Lac forms comparably shorter, straighter, more rigid assemblies consistent with previous observations (e.g. Knowles et al., 2007; Lara et al., 2011; Nicoud et al., 2015; Sweers et al., 2012). The Lyz and β-Lac images also display higher background noise compared to the images of α-Syn fibrils, which may reflect their overall less efficient fibril assembly reaction conditions compared to α-Syn. Importantly however, all of the samples showed well-dispersed fibril particles that can be individually measured after the brief stirring treatment, as the samples did not show strong propensity for clumping on the surface substrates.

The samples were then continuously stirred for up to 15 days and 1-5 µl samples (see Materials and Methods) were taken out periodically and imaged using AFM to visualise their fragmentation under mechanical perturbation (**Fig. 2**). For each sampling time-point, an identical AFM specimen preparation procedure was used for each amyloid type, and 20 µm x 20 µm surface areas were imaged at 2048 x 2048 pixels resolution in order to enable quantitative analysis of individual fibril particles as previously described (Xue, 2013; Xue et al., 2009b). In total, fragmentation of two independent fibril samples was followed for each fibril type, and 171 images with at least 300 particles for each sample and time point were analysed, giving a total dataset containing physical measurements of more than 220,000 individual fibril particles for the three amyloid types (**Supplementary Table S1**).

Quantitative single-particle measurements of fibril length and height distributions (**Fig. 3**, leftmost column corresponding to images in **Fig. 2**. leftmost column) reveal that the fibrils have substantially different initial dimensions. Analysis of their height distributions shows that the initial fibril heights, indicative of the width of the fibrils, are around 7 nm for α-Syn fibrils, and around 3 nm for both β-Lac and Lyz fibrils. The initial length distributions for the different fibril types were also dissimilar, with both Lyz and α-Syn forming fibrils of up to ~10 µm in length whereas β-Lac formed shorter particles with lengths of up to ~2 µm under the conditions employed.

Qualitative inspection of the AFM images throughout the experiment (**Fig. 3**) showed that the amyloid fibrils were fragmented into much smaller particles under the applied mechanical perturbation (**Fig. 2** and **Fig. 3**) as expected. However, the rate of division and shortening of the particles' lengths was seen to differ between the three different fibril types analysed (**Fig. 3** and **Supplementary Fig. S2**). Analysis of the time evolution of the fibril height and length distributions obtained by quantification of individual particles in the AFM images over the course of the experiment confirmed that fibril fragmentation did not cause detectable changes in fibril morphology and fibril width through lateral association and dissociation. Average fibril heights in the AFM

images, indicative of fibril widths, remained consistent throughout the experiment for Lyz and α-Syn. The same was also largely observed for β-Lac, with the exception that a small second population of taller polymers at the very end of the fragmentation time-course after 432000 s were exhibited (height graphs in **Fig. 3** and **Supplementary Fig. S2**). Hence the division of the fibrils under mechanical perturbation applied has resulted in a shortening of average fibril length.

To confirm that the changes in fibril length by fibril division did not cause disaggregation or release of monomer/small oligomers (e.g. dimers), we next determined the residual monomer concentration of the samples. For each fibril type, aggregates were pelleted by centrifugation (75k rpm, 15 min) after fragmentation time-course and the presence of monomer in the supernatants was quantified by SDS-PAGE. The comparison between the initial samples and those fragmented over two weeks showed no substantial changes in the protein composition of the supernatants, with differences of less than 2% for all amyloid systems analysed (Lyz: 1.4%, β-Lac: <1%, and α-Syn: 1.3%, **Supplementary Fig. S3**). These data confirmed that the time-dependent imaging experiments we carried out pertain almost exclusively to the fibril division processes along the length of the pre-formed fibrils, and therefore, contain valuable information on their division rates and their stability to division.

Time evolution of fibril length distributions converges to time-independent, characteristic, self-similar length distribution shapes

The fibril samples formed from different protein precursors have different initial length distributions (as seen in **Fig. 2** and **Fig. 3**). However, fibril division is itself a strongly length-dependent process (Xue and Radford, 2013) as short fibril particles will be more resistant towards division compared to longer particles, irrespectively of any differences in the intrinsic stability of the different fibril types to division. Therefore, to compare the stability of amyloid fibrils with different suprastructures and

length distributions towards division, a new approach to extract information intrinsic to each fibril type independent of their experimentally different initial length distributions must be developed. Consequently, in parallel with the experiments described above, we mathematically analysed the division equation of amyloid fibrils so that key information on the stability of amyloid fibrils to division could be resolved. We first describe the division of amyloid fibrils mathematically using a continuous framework based on the partial differential equation (PDE) Eq. (1). Since the number of monomers inside a fibril observed in the image data is large, typically in the order of 10^2 or more, we assumed continuous variables *x* and *y* that correspond to the length of fibrils (for example as defined in **Fig 1b** where y is the length of the parent fibril and x is the length of one of the daughter fibrils). This approach has the advantage that the infinite set of ordinary differential equations (ODEs) normally used to describe the length-dependent division processes (e.g. Knowles et al., 2009; Xue et al., 2008; Xue and Radford, 2013) can now be collapsed into a single continuous PDE that can be treated analytically (see Supplemental Information for details). Denoting *u(t,x)* as the distribution of fibrils of length *x* at time *t* in number concentration units (e.g. Molar units), Eq. (1) is the mathematical translation of the pure division model described by the schematics in **Fig.1b-d**, where we assume any parent fibril can divide into two daughters, and the end-end reattachment rate of daughter fibrils is negligible (Hill, 1983):

$$\frac{\partial}{\partial t}u(t,x) = -\alpha_0(\alpha x)^{\gamma}u(t,x) + 2\int_{y=x}^{\infty}\frac{1}{y}\kappa_0\left(\frac{x}{y}\right)\alpha_0(\alpha x)^{\gamma}u(t,y)dy$$

Eq. (1)

In Eq. (1), $\frac{\partial}{\partial t}u(t,x)$ denotes the time (t) evolution of the concentration of fibrils with length *x*. Here, we model the total division rate constant of fibrils of size *x* using the power law $\alpha_0(\alpha x)^{\gamma}$, which we denote as $B(x)$ (Hill, 1983) (see Supplementary Information), where α_0 is a constant unit reference we set to 1 s^{-1}. The first term in Eq (1), therefore, denotes the rate of loss of fibrils with length *x* by division into smaller fibrils. The probability that after dividing, a given parent fibril of length *y* gives rise to a daughter fibril fragments of length *x* and *y-x* depends on the ratio of the lengths (*x/y*) (Xue

and Radford, 2013) and is given by the probability density function $\frac{1}{y}\kappa_0\left(\frac{x}{y}\right)$. The second integral term in Eq. (1), therefore, denotes the total gain of fibrils with length *x* by division of all fibrils with length *y* that are larger than *x*. Interestingly, Eq. (1) describes a fundamental division process that is mathematically analogous to the division of molecules, macroscopic materials and cells (Escobedo et al., 2005; Robert et al., 2014), and we have mathematically proven that its behaviour is entirely and uniquely dictated by three properties: α that describes the magnitude of the division rate constant, γ that describes the fibril length dependence of the division rate constant, and κ_0 that describes the probability of division at any given position along a fibril, also called the fragmentation kernel (Doumic et al., 2018). We then proceeded to solve Eq. (1) analytically with regard to α, γ and κ_0 using theoretical results shown in (Escobedo et al., 2005) and (Doumic et al., 2018) (see Supplementary information). From our solution, we note four key predictive insights that emerged from our analysis (**Fig. 4**).

Firstly, we note that given enough time, the decay of the average fibril length will converge to the same rate independently of the initial fibril length distributions. This result comes from that after a sufficiently long time, the reduction of average length of the fibril length distribution can be described as a power law versus time (Eq. 2, see Supplementary Information):

$$\mu(t) = C \cdot t^{-1/\gamma} \qquad \text{Eq. (2)}$$

where *C* is a constant. As seen in Eq. (2), the experimentally observable average length of a sample, $\mu(t)$, is predicted to tend towards a straight line when plotted on a log-log plot with the slope of the line representing -1/γ (Eq. 2, black line in **Fig. 4b**) because the long-time behaviour of Eq. (1) can be described as a power law.

Secondly, we note that given enough time, the fibril length distribution will converge to the same shape independently of the initial state of the fibril length distribution. After a sufficiently long time ($t \gg t_0$), the distribution of fibril-lengths tends towards a time-independent distribution shape, $g(x_g)$, that scales only with *t* and γ, but does not depend on the initial length distribution (Eq. (3) and Supplementary Information).

$$g(x_g) \approx f(t,x) \cdot t^{-\frac{1}{\gamma}}, \qquad x_g = xt^{\frac{1}{\gamma}}, \qquad For\ any\ t \gg t_0$$

Eq. (3)

where *f(t, x)* are experimentally measured length distributions. This point is of key importance for characterising and predicting fibril division processes because it establishes that for any fibril type under certain conditions: 1) a distinct fibril length distribution shape (**Fig. 4a**) will be reached independently of the initial fibril length distribution, and 2) the length distribution and the average length will shrink as function of time in a predictive manner as fibrils continue to divide (e.g. the black line in **Fig. 4b** for the mean length) but the shape of the distribution will not change as function of time, i.e. the length distribution can be rescaled to the same $g(x_g)$ using Eq. (3) at any time *t* along the black line in **Fig. 4b** if *t* is sufficiently large. We refer to the distributions with the scaling property and shape invariance property as 'self-similar length distributions' (**Fig. 4a**).

The existence of a self-similar length distribution that is initial length distribution-independent and shape invariant over time, as well as the predictable decay of fibril lengths as fibrils divide (e.g. the reduction of the average length in **Fig. 4b**) can be seen as a characteristic behaviour specific to individual fibril types under distinct conditions. This fibril division behaviour can, therefore, be classed as a type of intrinsic dynamic stability of the fibrils. One way to visualise this property is shown in **Fig. 4b** represented by the black line, here referred to as the fibril type's 'asymptotic line' under the conditions applied. Any fibril populations above this line are relatively unstable and will

rapidly divide, pushing the average length towards the line (red and yellow coloured near-vertical arrows showing rapid decay of unstable fibril lengths). In contrast, any fibril populations below this line are comparatively stable or metastable and will only slowly evolve towards the line through division (green to blue coloured near-horizontal arrows showing slow decay of stable fibril lengths towards the black line). Importantly, this result also indicates that the dynamic stability of fibrils to division represented by the asymptotic line: 1) can be determined from experimental data, 2) is intrinsic to fibril type and conditions applied, and 3) can be compared independently of varied starting fibril length distributions, if the characteristic self-similar length distributions that contain information about the intrinsic dynamic stability of the fibrils is reached (e.g. the asymptotic line is reached in an experiment running for sufficiently long length of time).

Thirdly, we note that the probability of division in the centre of a fibril as compared to the shedding of small particles from fibril edge can be evaluated from the experiments. The self-similar length distributions contain information about κ_0. **Fig. 4c** shows how different self-similar fibril length distributions are indicative of different κ_0 probability functions. As seen in **Fig. 4c**, a κ_0 indicative of fibril types that are more likely to divide in the middle will result in fibril length distributions with a distinct peak and low relative population of small fragments. In contrast, a κ_0 indicative of fibril types and conditions that promote equal likelihood of division along the fibril or even favouring the shedding of fragments from fibril edges will result in self-similar fibril length distributions that have large relative population of small fibril fragments that may possess enhanced cytotoxic and/or infective potential compared to κ_0 favouring division in the centre of the fibrils.

Finally, the dynamic stability of fibrils to division, their propensity to break at different lengths, can be determined. The first order division rate constant $B(x) = \alpha_0(\alpha x)^\gamma$ that describes the division of the fibrils as a function of their length x can be directly evaluated from the self-similar length distribution and γ (see Eq. 2) when $t>>t_0$ (see Supplementary information and Eq SI.21) where t_0 is

the start of the experiment. Thus, the division rate constant *B(x)* can be determined from experimentally observing how fibril length distributions change with time when the self-similar fibril length distribution is obtained, and they are important parameters for defining and comparing the fibrils intrinsic dynamic stability to division. The effect of different values of α and γ on fibril stability is visualised in **Fig. 4d** and **Fig. 4e** as characteristic the asymptotic line plotted in log-log plots of average length versus time. The enumeration of the asymptotic line described by *B(x)* will subsequently enable direct quantitative comparison of the fibrils' stabilities towards division.

The division properties of amyloid fibrils can be obtained from image data and their complex stability to division can be compared

Applying the results of the mathematical analysis to the experimental AFM image data sets, the parameters γ, α, and the characteristic self-similar length-distributions $g(x_g)$ indicative of κ_0 can be extracted and meaningfully compared as a measure of the fibrils' intrinsic stability to division. We first determined the γ values for each of the fibril types, by globally fitting a variant of Eq. (2) to the time evolution of average fibril length (see Materials and Methods, **Fig. 5**). We also reanalysed previously published data set on β_2m fibril fragmentation under the same mechanical perturbation conditions (Xue and Radford, 2013) using our new theoretical results above and included the reanalysis in the comparison.

The constant γ was determined from least-squares fitting of our analytical result to the data (Materials and Methods). The power law relationship (Eq. 2) parameterised with γ determined by global analysis was visualised on a log-log plot of mean fibril length vs. time in **Fig. 5**, together with the measured mean fibril lengths. The resulting γ values are listed in **Table 1**. A γ value of 1 would suggest that the division rate of fibrils is only dependent on the number of division sites per fibril, which is linearly

related to the number of monomers in the fibrils and in turn to the length of the fibrils. However, the γ values for α-Syn, β-Lac and β_2m are all significantly larger than 1, indicating highly length dependent microscopic division rates for division sites in these fibril types. Of the four fibril types analysed, the division of Lyz fibrils yielded a γ value closest to 1. This suggests the division rates for Lyz fibrils may only depend on the number of available division sites along the fibrils. β-Lac fibrils yielded the highest γ value of the fibril types analysed. This demonstrates that β-Lac fibril fragmentation is highly length-dependent, and small β-Lac fibril fragments are more resistant to further fragmentation compared with the other fibril types. This behaviour may corroborate with an increased lateral association of small β-Lac fibril fragmentation fragments observed on the height distributions at the end of the time-course experiments (height graphs in **Fig. 3** and **Supplementary Fig. S2**). As seen in **Fig. 5**, the later time points for all of our fibril types follow a straight line on the log-log plots (solid section of the fitted lines in **Fig. 5**), indicating that the self-similar length distributions, and hence the asymptotic line, were sufficiently reached in all cases. The analysis also revealed that all of the fibril types analysed approached the self-similar length distribution shapes in less than 5 hr, with the exception of the Lyz samples that reached the self-similar distribution in approximately 24 hr.

The α values were subsequently calculated (listed in **Table 1**) with equations Eq. (S21) using all of the fibril length distributions at time points post reaching the near-characteristic self-similar distribution shapes (represented by the solid lines in **Fig. 5**). Once both α and γ values have been extracted from the length-distribution data, the division rate constant $B(x)$ can be obtained for fibrils of any length x. **Table 1** shows the division rate constant calculated for fibrils of 100 nm. The asymptotic line for the fibrils types characterised by the division rate constant $B(x)$ (**Fig. 6b**) or by fibril mean length (**Fig. 6a**) as function of time was also visualised and compared independently of initial fibril length, showing that α-Syn and Lyz fibrils fragments fastest at long-times under the mechanical perturbation applied, suggesting that these fibrils were less stable than the β-Lac and β_2m fibrils.

Next, we determined the shape of the self-similar length distributions for each fibril type by rescaling the experimental length distributions to $g(x_g)$ with Eq. (3) using the γ values obtained above. As with the evaluation of α values, only time points where the length distributions closely approached the self-similar length distribution (time points in the section represented by the solid lines in **Fig. 5**) were averaged to obtain $g(x_g)$ for each fibril type (**Supplementary Fig. S4**). **Fig. 6c** shows how the self-similar length distribution shapes compare with each other at extended times (2 weeks) when calculated using $g(x_g)$ (**Supplementary Fig. S4**) with Eq. (3). As seen in Fig 6c, Lyz fibrils tend to produce high relative populations of small particles less than 100 nm long followed by α-Syn and then β_2m. On the other hand, the division of β-Lac fibrils resulted in a lower relative population of small particles over the same long time scale used for the other fibril types.

Finally, to validate our model and the predictive power of our approach, we performed direct simulations of the fibril division time-course (**Fig. 7**) using only the individual sets of division parameters obtained for each of our fibril types. For each simulation, we used the initial experimental length distributions (dashed lines in **Fig. 7**) directly as the starting points for the simulations. The large set of ordinary differential equations describing the chemical master equation for the system (Xue and Radford, 2013) was then solved to see whether our analytical model was able to predict the full division behaviour and the time evolution of the fibril length distributions for each fibril type. As seen in **Fig. 7**, the result of the numerical simulations based on our results show remarkable agreement with the experimental data. This unequivocal result validated the fact that the set of three properties γ, α, and κ_0 are indeed capable of fully and uniquely describing the complex amyloid division processes, and the enumeration of these properties yield valuable insights. Such insights allow meaningful comparison of the amyloid fibrils' intrinsic stability to division.

DISCUSSION

The understanding of the properties that underline the biological activities of amyloid nano-structures, such as their cytotoxic and infectious potentials, is crucial for the understanding of why some amyloid is associated with devastating human diseases. The division of amyloid fibrils, for example through fibril fragmentation by mechanical perturbation (Xue et al., 2008; Xue and Radford, 2013), enzymatic action (Chernoff et al., 1995; Glover and Lindquist, 1998) or other cellular or environmental perturbations, is a key step in their life-cycle that results in the exponential growth in the number of amyloid particles. Simultaneously, daughter particles resulting from the division of parent fibrils cause a reduction in the overall size distribution as division proceeds. These two consequences of division are undoubtedly linked to the enhancement of the cytotoxic and infectious potentials of disease-associated amyloid (Marchante et al., 2017; Xue et al., 2009a). The amyloid fibrils' resistance to division, i.e. the stability of the amyloid fibrils to division, rationalises these two fundamental requirements for pathogenicity associated with amyloid. Akin to uncontrolled division of cells or any pathogenic microorganisms, the division step in the amyloid life cycle (**Fig. 1**) could be a key determinant in their overall potential to be associated with properties in the amyloid and prion associated pathology.

Here, we have developed a theory, as well as an experimental approach utilising our theoretical insights to resolve the amyloid fibrils' dynamic stability to division. These represent a step forward in how we are able to study the amyloid fibril division processes such as in fibril fragmentation and prion propagation, essentially the replication step in the amyloid lifecycle. It also allows the direct comparison between amyloid particles of different molecular types and quantifies the difference in division and stability between those that are and are not disease associated. Specifically, we have applied our theoretical results to the comparison of a diverse set of amyloid assemblies consisting of

human α-Syn (a neurodegenerative disease-associated amyloid, sample formed under physiological solution conditions), human β_2m (a systemic amyloidosis disease-associated amyloid, sample formed under acidic pH, data from Xue and Radford, 2013), bovine β-Lac and hen egg white Lyz (later two cases are both biophysical model systems not directly related to human disease but converted to amyloid when subjected to heating in acidic pH). By fully analysing and comparing their division behaviour, which is uniquely described by the triplet of parameters (α, magnitude of the division rate constant, γ, fibril length dependence of the division rate constant, and κ_0, probability of division at any given position along a fibril) under identical mechanical perturbation for long timescales using our approach, we show a remarkable difference in the stability of these different amyloid assemblies relative to each other and how they divide (summarised in **Fig. 8**). Interestingly, for the four fibril types we included here, considering the division rate constant B with their cross-sectional area, the disease-associated human α-Syn fibrils demonstrate lowest overall stability to division followed by Lyz, human β_2m and finally β-Lac particles that are most stable towards division (**Fig 8.** last row). Based on the comparison of the α and γ parameters that together describe the division rates *B(x)*, the likelihood that small α-Syn particles (<100 nm long) will divide is similar to that of Lyz particles of identical length despite having more than double the mean width (and thus around four times bigger cross-sectional area, **Table 1** and **Fig. 8**). More importantly, the division of α-Syn particles also results in a larger relative concentration of small particles compared to β_2m and β-Lac. These results show that human α-Syn amyloid fibrils are relative unstable assemblies capable of a more rapid shedding of small particles that could well possess enhanced cytotoxic and infectious potentials (Peelaerts et al., 2015) through division compared with the other fibril types investigated here. Thus, our results also directly suggest a testable causality link between the low stability of α-Syn fibrils to division and recent observations that human α-Syn may behave in a prion-like manner in cell to cell propagation and their cytotoxicity (Steiner et al., 2018).

Since the division of amyloid fibrils is an integral part in the propagation of the amyloid conformation (**Fig. 1**), the nanoscale materials properties of amyloid underpin processes which drive the

proliferation of amyloid, as well as their varied roles in biology. Therefore, it is important to appreciate the suprastructural properties of amyloid (e.g. clustering, bundling, twist, stiffness, width distribution, orientation distribution, and length distribution etc) at mesoscopic (nanometre to micrometre) length scales, as these properties will influence how individual amyloid fibrils divide. Our data show that despite all amyloid consisting of a cross-beta core structure, their ability to resist division through fragmentation promoted by mechanical perturbation varies strongly between fibril types. Since the stability of amyloid fibrils to division will depend on their suprastructural properties, which in turn depend on their precise structure at atomic level, mesoscopic level structural properties may well be the missing link between amyloid structure and the varied biological effects and consequences that different amyloid types evoke under different conditions. While the results reported here reveal the breakage behaviour of fibril populations, future advances in AFM imaging may allow either individual polymorphs in a fibril population to be distinguished or individual fibrils to be tracked in real-time, further revealing how fibrils divide as individuals. Thus, it should be possible to generate a structure activity relationship correlating the suprastrucutral properties of amyloid, their ability to divide, and their cytotoxic and/or infectious potentials. Understanding this structure activity relationship for amyloid assemblies could lead to the design of bio-safe polymers with tuned mechanical and nanomaterials properties as well as rationalise the disease-associated properties of amyloid structures.

Analogous to the diverse response of soluble folded proteins towards unfolding by chemical denaturants, thermal melting and mechanical force etc., the stability of amyloid fibrils could also vary depending on the nature of the perturbation. Indeed, amyloid fibrils may break down in the presence of chemical, thermal or enzymatic action (Baldwin et al., 2011; Chernoff et al., 1995; Glover and Lindquist, 1998; Knowles et al., 2007; Shammas et al., 2011; Surmacz-Chwedoruk et al., 2014), and their relative resistance or stability to different stresses, including those associated with physiological changes involved in human disorders, is not known. In particular, understanding how enzymatic action by molecular chaperones such as Hsp104 or ClpB promote amyloid division, degradation

and/or propagation of amyloid conformation (Chernova et al., 2017; Scior et al., 2016) in relevant cases may be key in resolving the complex behaviour of the amyloid lifecycle in a biological context. In summary, the combined theoretical and experimental work we report here will enable the characterisation and comparison of the amyloid division processes and the relative stabilities of amyloid assemblies. Both properties are fundamental in understanding the lifecycle of disease-associated amyloid as well as the normal roles of functional amyloid in biology.

LIMITATIONS OF THE STUDY

The division model (assumptions illustrated in **Fig. 1**) does not take into account the possibilities that newly created fibril ends by division may be more dynamic, disordered, and/or being 'sticky ends' in their interactions with other fibril ends or surfaces compared with established fibril ends for elongation. The results reported here reveal the overall breakage behaviour of the fibril populations, as our experiments may contain a mixture of similar but nevertheless different polymorphs that could not be readily distinguished in our images. Future advances in AFM imaging allowing either individual polymorphs in a fibril population to be distinguished or individual fibrils to be tracked in real-time will resolve breakage behaviour of individual fibril polymorphs. The model assumptions and limitations may also leave scope for improvements in the model to be pursued in future work by the field.

RESOURCE AVAILABILITY

Lead contact

Wei-Feng Xue (w.f.xue@kent.ac.uk).

Materials availability

This study did not generate new unique reagents

Data and code availability

The published article includes all datasets generated and analysed during this study. List of all (over 220 000) raw fibril lengths and associated analysis code supporting the current study are available from the corresponding author on request.

MATERIAL AND METHODS

All materials and methods can be found in the accompanying Transparent Methods supplemental file

ACKNOWLEDGEMENTS

We thank the members of the Xue group, and the Kent Fungal Group for helpful comments throughout the preparation of this manuscript, and Ian Brown for technical support. We also thank Sheena Radford for insightful discussions, as well as help and support on the reanalysis of β_2-

microglobuling fragmentation dataset. This work was supported by funding from INRIA (W.-F.X and M.D), the European Research Council (ERC) Starting Grant number 306321, SKIPPERAD (M.D) the Biotechnology and Biological Sciences Research Council (BBSRC) UK grants BB/J008001/1 (W.-F.X) as well as BB/F016719/1 (D.M.B), and The Wellcome Trust grant 209171/Z/17/Z (D.M.B)

AUTHOR CONTRIBUTIONS

D.M.B. designed the research, conducted the experiments, and analysed the data. M.T. designed the research, developed the theory, wrote the analytical software tools, and analysed the data. R.M. and T.J.P. conducted the experiments. D.P.S. provided reagents and methods, and analysed the data. M.F.T. designed the research and analysed the data. M.D. designed the research, developed the theory and analysed the data. W.F.X. designed the research, wrote the analytical software tools, developed the theory, analysed the data, and managed the research. The manuscript was written through contributions of all authors.

DECLARATION OF INTERESTS

The authors declare no conflicts of interest.

REFERENCES

Aguzzi, A., Heikenwalder, M., and Polymenidou, M. (2007). Insights into prion strains and neurotoxicity. Nat Rev Mol Cell Biol *8*, 552-561.

Ankarcrona, M., Winblad, B., Monteiro, C., Fearns, C., Powers, E.T., Johansson, J., Westermark, G.T., Presto, J., Ericzon, B.G., and Kelly, J.W. (2016). Current and future treatment of amyloid diseases. J Intern Med *280*, 177-202.

Baldwin, A.J., Knowles, T.P., Tartaglia, G.G., Fitzpatrick, A.W., Devlin, G.L., Shammas, S.L., Waudby, C.A., Mossuto, M.F., Meehan, S., Gras, S.L., *et al.* (2011). Metastability of native proteins and the phenomenon of amyloid formation. J Am Chem Soc *133*, 14160-14163.

Barritt, J.D., Younan, N.D., and Viles, J.H. (2017). N-Terminally Truncated Amyloid-beta(11-40/42) Cofibrillizes with its Full-Length Counterpart: Implications for Alzheimer's Disease. Angew Chem Int Ed Engl *56*, 9816-9819.

Berson, J.F., Theos, A.C., Harper, D.C., Tenza, D., Raposo, G., and Marks, M.S. (2003). Proprotein convertase cleavage liberates a fibrillogenic fragment of a resident glycoprotein to initiate melanosome biogenesis. J Cell Biol *161*, 521-533.

Bleem, A., and Daggett, V. (2017). Structural and functional diversity among amyloid proteins: Agents of disease, building blocks of biology, and implications for molecular engineering. Biotechnol Bioeng *114*, 7-20.

Breydo, L., and Uversky, V.N. (2015). Structural, morphological, and functional diversity of amyloid oligomers. FEBS Lett *589*, 2640-2648.

Brundin, P., and Melki, R. (2017). Prying into the Prion Hypothesis for Parkinson's Disease. J Neurosci *37*, 9808-9818.

Buell, A.K., Galvagnion, C., Gaspar, R., Sparr, E., Vendruscolo, M., Knowles, T.P., Linse, S., and Dobson, C.M. (2014). Solution conditions determine the relative importance of nucleation and growth processes in alpha-synuclein aggregation. Proc Natl Acad Sci U S A *111*, 7671-7676.

Cappai, R., Leck, S.L., Tew, D.J., Williamson, N.A., Smith, D.P., Galatis, D., Sharples, R.A., Curtain, C.C., Ali, F.E., Cherny, R.A., *et al.* (2005). Dopamine promotes alpha-synuclein aggregation into SDS-resistant soluble oligomers via a distinct folding pathway. FASEB J *19*, 1377-1379.

Chapman, M.R., Robinson, L.S., Pinkner, J.S., Roth, R., Heuser, J., Hammar, M., Normark, S., and Hultgren, S.J. (2002). Role of Escherichia coli curli operons in directing amyloid fiber formation. Science *295*, 851-855.

Chernoff, Y.O., Lindquist, S.L., Ono, B., Inge-Vechtomov, S.G., and Liebman, S.W. (1995). Role of the chaperone protein Hsp104 in propagation of the yeast prion-like factor [psi+]. Science *268*, 880-884.

Chernova, T.A., Wilkinson, K.D., and Chernoff, Y.O. (2017). Prions, Chaperones, and Proteostasis in Yeast. Cold Spring Harb Perspect Biol *9*, a023663.

Cox, B., Ness, F., and Tuite, M. (2003). Analysis of the generation and segregation of propagons: entities that propagate the [PSI+] prion in yeast. Genetics *165*, 23-33.

Derdowski, A., Sindi, S.S., Klaips, C.L., DiSalvo, S., and Serio, T.R. (2010). A size threshold limits prion transmission and establishes phenotypic diversity. Science *330*, 680-683.

Dobson, C.M. (1999). Protein misfolding, evolution and disease. Trends Biochem Sci *24*, 329-332.

Doumic, M., Escobedo, M., and Tournus, M. (2018). Estimating the division rate and kernel in the fragmentation equation. Ann I H Poincare-An *35*, 1847-1884.

Escobedo, M., Mischler, S., and Ricard, M.R. (2005). On self-similarity and stationary problem for fragmentation and coagulation models. Ann I H Poincare-An *22*, 99-125.

Glover, J.R., and Lindquist, S. (1998). Hsp104, Hsp70, and Hsp40: a novel chaperone system that rescues previously aggregated proteins. Cell *94*, 73-82.

Hill, T.L. (1983). Length dependence of rate constants for end-to-end association and dissociation of equilibrium linear aggregates. Biophys J *44*, 285-288.

Hu, B., Shen, Y., Adamcik, J., Fischer, P., Schneider, M., Loessner, M.J., and Mezzenga, R. (2018). Polyphenol-Binding Amyloid Fibrils Self-Assemble into Reversible Hydrogels with Antibacterial Activity. ACS Nano *12*, 3385-3396.

Hu, X., Crick, S.L., Bu, G., Frieden, C., Pappu, R.V., and Lee, J.M. (2009). Amyloid seeds formed by cellular uptake, concentration, and aggregation of the amyloid-beta peptide. Proc Natl Acad Sci U S A *106*, 20324-20329.

Jakhria, T., Hellewell, A.L., Porter, M.Y., Jackson, M.P., Tipping, K.W., Xue, W.F., Radford, S.E., and Hewitt, E.W. (2014). beta2-microglobulin amyloid fibrils are nanoparticles that disrupt lysosomal membrane protein trafficking and inhibit protein degradation by lysosomes. J Biol Chem *289*, 35781-35794.

Khan, T., Kandola, T.S., Wu, J., Venkatesan, S., Ketter, E., Lange, J.J., Rodriguez Gama, A., Box, A., Unruh, J.R., Cook, M., *et al.* (2018). Quantifying Nucleation In Vivo Reveals the Physical Basis of Prion-like Phase Behavior. Mol Cell *71*, 155-168 e157.

Knowles, T.P., and Buehler, M.J. (2011). Nanomechanics of functional and pathological amyloid materials. Nat Nanotechnol *6*, 469-479.

Knowles, T.P., Fitzpatrick, A.W., Meehan, S., Mott, H.R., Vendruscolo, M., Dobson, C.M., and Welland, M.E. (2007). Role of intermolecular forces in defining material properties of protein nanofibrils. Science *318*, 1900-1903.

Knowles, T.P., Vendruscolo, M., and Dobson, C.M. (2014). The amyloid state and its association with protein misfolding diseases. Nat Rev Mol Cell Biol *15*, 384-396.

Knowles, T.P., Waudby, C.A., Devlin, G.L., Cohen, S.I., Aguzzi, A., Vendruscolo, M., Terentjev, E.M., Welland, M.E., and Dobson, C.M. (2009). An analytical solution to the kinetics of breakable filament assembly. Science *326*, 1533-1537.

Lara, C., Usov, I., Adamcik, J., and Mezzenga, R. (2011). Sub-persistence-length complex scaling behavior in lysozyme amyloid fibrils. Phys Rev Lett *107*, 238101.

Larsen, P., Nielsen, J.L., Dueholm, M.S., Wetzel, R., Otzen, D., and Nielsen, P.H. (2007). Amyloid adhesins are abundant in natural biofilms. Environ Microbiol *9*, 3077-3090.

Lee, Y.J., Savtchenko, R., Ostapchenko, V.G., Makarava, N., and Baskakov, I.V. (2011). Molecular structure of amyloid fibrils controls the relationship between fibrillar size and toxicity. PLoS One *6*, e20244.

Li, D., Jones, E.M., Sawaya, M.R., Furukawa, H., Luo, F., Ivanova, M., Sievers, S.A., Wang, W., Yaghi, O.M., Liu, C., *et al.* (2014). Structure-based design of functional amyloid materials. J Am Chem Soc *136*, 18044-18051.

Lin, H.K., Boatz, J.C., Krabbendam, I.E., Kodali, R., Hou, Z., Wetzel, R., Dolga, A.M., Poirier, M.A., and van der Wel, P.C.A. (2017). Fibril polymorphism affects immobilized non-amyloid flanking domains of huntingtin exon1 rather than its polyglutamine core. Nat Commun *8*, 15462.

Lorenzen, N., Cohen, S.I., Nielsen, S.B., Herling, T.W., Christiansen, G., Dobson, C.M., Knowles, T.P., and Otzen, D. (2012). Role of elongation and secondary pathways in S6 amyloid fibril growth. Biophys J *102*, 2167-2175.

Mankar, S., Anoop, A., Sen, S., and Maji, S.K. (2011). Nanomaterials: amyloids reflect their brighter side. Nano Rev *2*, 6032.

Marchante, R., Beal, D.M., Koloteva-Levine, N., Purton, T.J., Tuite, M.F., and Xue, W.F. (2017). The physical dimensions of amyloid aggregates control their infective potential as prion particles. Elife *6*, e27109.

Meinhardt, J., Sachse, C., Hortschansky, P., Grigorieff, N., and Fandrich, M. (2009). Abeta(1-40) fibril polymorphism implies diverse interaction patterns in amyloid fibrils. J Mol Biol *386*, 869-877.

Milanesi, L., Sheynis, T., Xue, W.F., Orlova, E.V., Hellewell, A.L., Jelinek, R., Hewitt, E.W., Radford, S.E., and Saibil, H.R. (2012). Direct three-dimensional visualization of membrane disruption by amyloid fibrils. Proc Natl Acad Sci U S A *109*, 20455-20460.

Nicoud, L., Lazzari, S., Balderas Barragan, D., and Morbidelli, M. (2015). Fragmentation of amyloid fibrils occurs in preferential positions depending on the environmental conditions. J Phys Chem B *119*, 4644-4652.

Paparcone, R., and Buehler, M.J. (2011). Failure of Abeta(1-40) amyloid fibrils under tensile loading. Biomaterials *32*, 3367-3374.

Peelaerts, W., Bousset, L., Van der Perren, A., Moskalyuk, A., Pulizzi, R., Giugliano, M., Van den Haute, C., Melki, R., and Baekelandt, V. (2015). alpha-Synuclein strains cause distinct synucleinopathies after local and systemic administration. Nature *522*, 340-344.

Robert, L., Hoffmann, M., Krell, N., Aymerich, S., Robert, J., and Doumic, M. (2014). Division in Escherichia coli is triggered by a size-sensing rather than a timing mechanism. BMC Biol *12*, 17.

Romero, D., Aguilar, C., Losick, R., and Kolter, R. (2010). Amyloid fibers provide structural integrity to Bacillus subtilis biofilms. Proc Natl Acad Sci U S A *107*, 2230-2234.

Sachse, C., Grigorieff, N., and Fandrich, M. (2010). Nanoscale flexibility parameters of Alzheimer amyloid fibrils determined by electron cryo-microscopy. Angew Chem Int Ed Engl *49*, 1321-1323.

Scior, A., Juenemann, K., and Kirstein, J. (2016). Cellular strategies to cope with protein aggregation. Essays Biochem *60*, 153-161.

Shammas, S.L., Knowles, T.P., Baldwin, A.J., Macphee, C.E., Welland, M.E., Dobson, C.M., and Devlin, G.L. (2011). Perturbation of the stability of amyloid fibrils through alteration of electrostatic interactions. Biophys J *100*, 2783-2791.

Shorter, J., and Lindquist, S. (2004). Hsp104 catalyzes formation and elimination of self-replicating Sup35 prion conformers. Science *304*, 1793-1797.

Sondheimer, N., and Lindquist, S. (2000). Rnq1: an epigenetic modifier of protein function in yeast. Mol Cell *5*, 163-172.

Steiner, J.A., Quansah, E., and Brundin, P. (2018). The concept of alpha-synuclein as a prion-like protein: ten years after. Cell Tissue Res *373*, 161-173.

Surmacz-Chwedoruk, W., Malka, I., Bozycki, L., Nieznanska, H., and Dzwolak, W. (2014). On the heat stability of amyloid-based biological activity: insights from thermal degradation of insulin fibrils. PLoS One *9*, e86320.

Sweers, K.K., van der Werf, K.O., Bennink, M.L., and Subramaniam, V. (2012). Atomic force microscopy under controlled conditions reveals structure of C-terminal region of alpha-synuclein in amyloid fibrils. ACS Nano *6*, 5952-5960.

Tanaka, M., Collins, S.R., Toyama, B.H., and Weissman, J.S. (2006). The physical basis of how prion conformations determine strain phenotypes. Nature *442*, 585-589.

Tipping, K.W., van Oosten-Hawle, P., Hewitt, E.W., and Radford, S.E. (2015). Amyloid Fibres: Inert End-Stage Aggregates or Key Players in Disease? Trends Biochem Sci *40*, 719-727.

Tornquist, M., Michaels, T.C.T., Sanagavarapu, K., Yang, X., Meisl, G., Cohen, S.I.A., Knowles, T.P.J., and Linse, S. (2018). Secondary nucleation in amyloid formation. Chem Commun (Camb) *54*, 8667-8684.

Tuite, M.F., and Serio, T.R. (2010). The prion hypothesis: from biological anomaly to basic regulatory mechanism. Nat Rev Mol Cell Biol *11*, 823-833.

Xue, W.F. (2013). Amyloid Fibril Length Quantification by Atomic Force Microscopy. In Bio-Nanoimaging Protein Misfolding & Aggregation, V.N. Uversky, and Y.L. Lyubchenko, eds. (Academic Press), pp. 17-25.

Xue, W.F. (2015). Nucleation: The Birth of a New Protein Phase. Biophys J *109*, 1999-2000.

Xue, W.F., Hellewell, A.L., Gosal, W.S., Homans, S.W., Hewitt, E.W., and Radford, S.E. (2009a). Fibril fragmentation enhances amyloid cytotoxicity. J Biol Chem *284*, 34272-34282.

Xue, W.F., Homans, S.W., and Radford, S.E. (2008). Systematic analysis of nucleation-dependent polymerization reveals new insights into the mechanism of amyloid self-assembly. Proc Natl Acad Sci U S A *105*, 8926-8931.

Xue, W.F., Homans, S.W., and Radford, S.E. (2009b). Amyloid fibril length distribution quantified by atomic force microscopy single-particle image analysis. Protein Eng Des Sel *22*, 489-496.

Xue, W.F., and Radford, S.E. (2013). An imaging and systems modeling approach to fibril breakage enables prediction of amyloid behavior. Biophys J *105*, 2811-2819.

Zeng, G., Vad, B.S., Dueholm, M.S., Christiansen, G., Nilsson, M., Tolker-Nielsen, T., Nielsen, P.H., Meyer, R.L., and Otzen, D.E. (2015). Functional bacterial amyloid increases Pseudomonas biofilm hydrophobicity and stiffness. Front Microbiol *6*, 1099.

FIGURE LEGENDS

Figure 1. Schematic illustration of fibril division in the amyloid lifecycle. *(a) The lifecycle of amyloid assembly where soluble monomeric protein (circles) are converted into the amyloid state with a cross-β conformation (the parallelograms). The coloured arrows represent the four main processes in amyloid assembly. Red arrows represent primary nucleation, which may occur as homogeneous nucleation in solution, heterogeneous nucleation at interfaces. Primary nucleation may also occur subsequent to liquid-liquid phase separation or phase transitions (Khan et al., 2018). Purple arrows represent secondary nucleation, which may occur as heterogeneous nucleation at surfaces presented by preformed aggregates. Blue arrows represent growth by elongation at fibril ends. Yellow arrows and box represent fibril division (e.g. fibril fragmentation or breakage). The arrows may represent consecutive reversible steps and the thickness of the arrows symbolizes the relative rates involved in the processes. (b) A simple model of fibril division, where a given parent fibril particle of length y divides to give rise to two daughter fibril particles of size x and y-x. The model does not otherwise identify the lineage of the individual fibrils. (c) The division model assumes that each parent fibril particle divides into exactly two daughter particles at each microscopic reaction step. (d) The division model assumes that the division rate for each microscopic step is identical as long as the resulting two particles have the same size.*

Figure 2. AFM imaging of amyloid fibrils undergoing fragmentation promoted by mechanical stirring. *Hen egg white Lyz, bovine milk β-Lac, and human α-Syn amyloid fibril samples (all 120 μM monomer equivalent concentration) were stirred for up to 15 days. Samples were taken out periodically, deposited on mica and imaged using AFM. Typical AFM images representing 10x10 μm surface areas are show together with 4x magnified insets. The scale bar represents 2 μm in all images.*

Figure 3. Fibril length and height distributions extracted from AFM images of the fibril undergoing fragmentation by mechanical perturbation. *Normalised length (upper row of each sample) and height (lower row of each sample) distributions of fibril particles corresponding to the same AFM images in* ***Fig. 2*** *are shown as histograms. The histograms are shown using the same length and height scales, respectively, for comparison.*

Figure 4. Illustration of the key insights emerging from the mathematical analysis of the division model. *The behaviour of the division equation Eq. (1) is entirely and uniquely dictated by a set of three properties: α, γ, and κ_0. Several key predictive insights emerged from the analytical solution of Eq. (1) with regard to these three properties. (a) The three example length distributions in the left panel can be rescaled to show the same distribution shape in the right panel, illustrating the concept of self-similar length distributions. (b) After a period of time, where the self-similar length distribution shape is reached. From this point, the reduction in the average length of the fibril length distribution can be described as a power law versus time. The decay of mean length of a sample is predicted to tend towards a straight line, the asymptotic line, when plotted on a log-log plot with the slope of the line representing $-1/\gamma$ (black line in b, d and e). The stability line with mean fibril lengths also does not depend on the initial length distribution (coloured lines in b). (c) The self-similar length distribution shape contains information about κ_0, which describes how likely a fibril will divide in the middle versus shedding a small fragment from the edge. A κ_0 indicative of fibril types that are more likely to divide in the middle will result in fibril length distributions with a distinct peak and low relative population of small fragments (dark green and light green curves). In contrast, κ_0 indicative of fibril types and conditions that promote equal likelihood of division along the fibril or even favour shedding of small fragments from fibril edges will result in self-similar fibril length distributions that have a larger relative population of small fibril fragments (yellow and orange curves) compared to κ_0 values favouring division in the centre of the fibrils. (d) and (e) illustrate how the black asymptotic*

line describing the decay of fibril lengths in (a) is dictated by the parameters α and γ, respectively. For each panel, the colour bar to the right illustrates the different properties associated with the colours in the panel (e.g. division in the centre vs. at the edge of a fibril for panel c, and division of a long vs. a short fibril in panel e)

Figure 5. Fitting the fibril division model to fibril length decay data extracted from AFM images. *The analytical solution of our division model shows the decay of average length as function of the gamma parameter in equation Eq. (2) and Eq. (4). Equation Eq. (4) was fitted to the decay of average fibril length during division for each of the fibril types analysed (including previously published data for β_2m fragmentation under the same mechanical perturbation conditions in Xue and Radford, 2013). The solid fitted lines represent the time regime where the length distributions closely approached the stability line and the self-similar distribution shape where Eq. (2) is valid (Materials and Methods).*

Figure 6. Comparing the stability towards division of different amyloid fibril types. *The decay of mean lengths (a), the division rate constants as function of fibril length (b), and the self-similar length distribution shapes (c) for hen egg Lyz (blue), bovine milk β-Lac (yellow), human α-Syn (red) and human β_2m (black, data from Xue and Radford, 2013) amyloid fibril samples undergoing division by fibril fragmentation under mechanical perturbation. All curves were calculated using α, γ, and $g(x_g)$ obtained from our analysis of the experimental AFM images. In (a), the thicker portion of the lines denote the time range where the characteristic self-similar length distribution shape is observed in the imaging experiments (i.e. corresponding to the time regime represented by the solid fitted lines in* ***Fig. 5****), and crosses are the experimental data points that have closely reached the self-similar distribution shapes shown in the same plot. In (b), the thicker portion of the lines denote the range of fibril lengths observed experimentally on the AFM images. In (c), the distributions were calculated using self-similar distributions $g(x_g)$ in* ***Supplementary Fig. S3*** *after two weeks.*

Figure 7. Validation of the division parameters α, γ and κ_0 and their predictive power. *Full direct simulation of fibril fragmentation processes using α, γ and κ_0 determined from the image data. For each fibril type, the initial normalised frequency distribution (dashed lines in top row) were used directly as the initial state for the simulations. The resulting simulated evolution of length distributions solely based on the calculated α and γ values and estimated shapes κ_0 (see Materials and methods) are compared with the experimental data show as histograms.*

Figure 8. Schematic summary of the fibril division properties and their consequences compared between each of the fibril types. *Comparison of the fibril division profiles reveal differences in the dynamical stability towards breakage for the four different types of amyloid fibrils, and suggest that disease-related amyloid has lowered stability towards breakage and increased likelihood of shedding smaller particles compared to amyloid not related to disease. In the illustrations, the fibril width, number and number of breakage symbols are not to scale and denote the relative rankings for the different properties.*

TABLES

Table 1. Parameters from the division analysis of the different fibril types

Sample	*γ ± SE*	*α / nm^{-1} (log α ± SE)*	*B (100 nm) / s^{-1} (log B ± SE)*	*Height (fibril width) / nm*

***α*-Syn**	2.0 ± 0.3	$2.6 \cdot 10^{-6}$ (-5.6 ± 0.2)	$9.2 \cdot 10^{-8}$ (-7.0 ± 0.3)	6.8 ± 0.6
***β*-Lac**	5.7 ± 0.8	$1.8 \cdot 10^{-4}$ (-3.7 ± 0.2)	$1.2 \cdot 10^{-10}$ (-9.9 ± 0.8)	3.0 ± 0.5
Lyz	1.7 ± 1.0	$9.4 \cdot 10^{-7}$ (-6.0 ± 0.9)	$2.0 \cdot 10^{-7}$ (-6.7 ± 1.0)	3.1 ± 0.4
β_2m*	3.4 ± 0.4	$5.6 \cdot 10^{-5}$ (-4.3 ± 0.3)	$2.5 \cdot 10^{-8}$ (-7.6 ± 0.4)	5.4 ± 0.6

* Reanalysis of data from Xue and Radford, 2013.

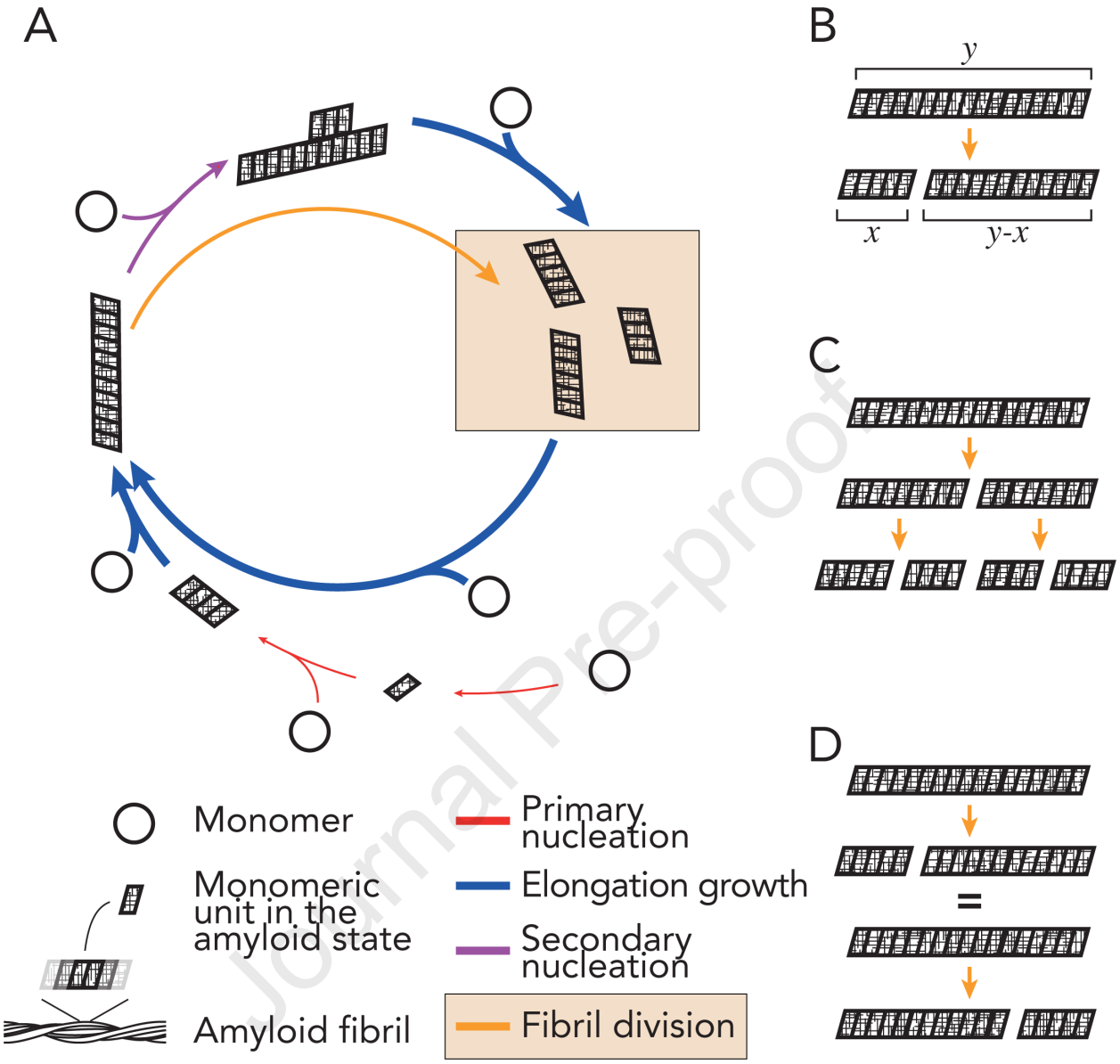

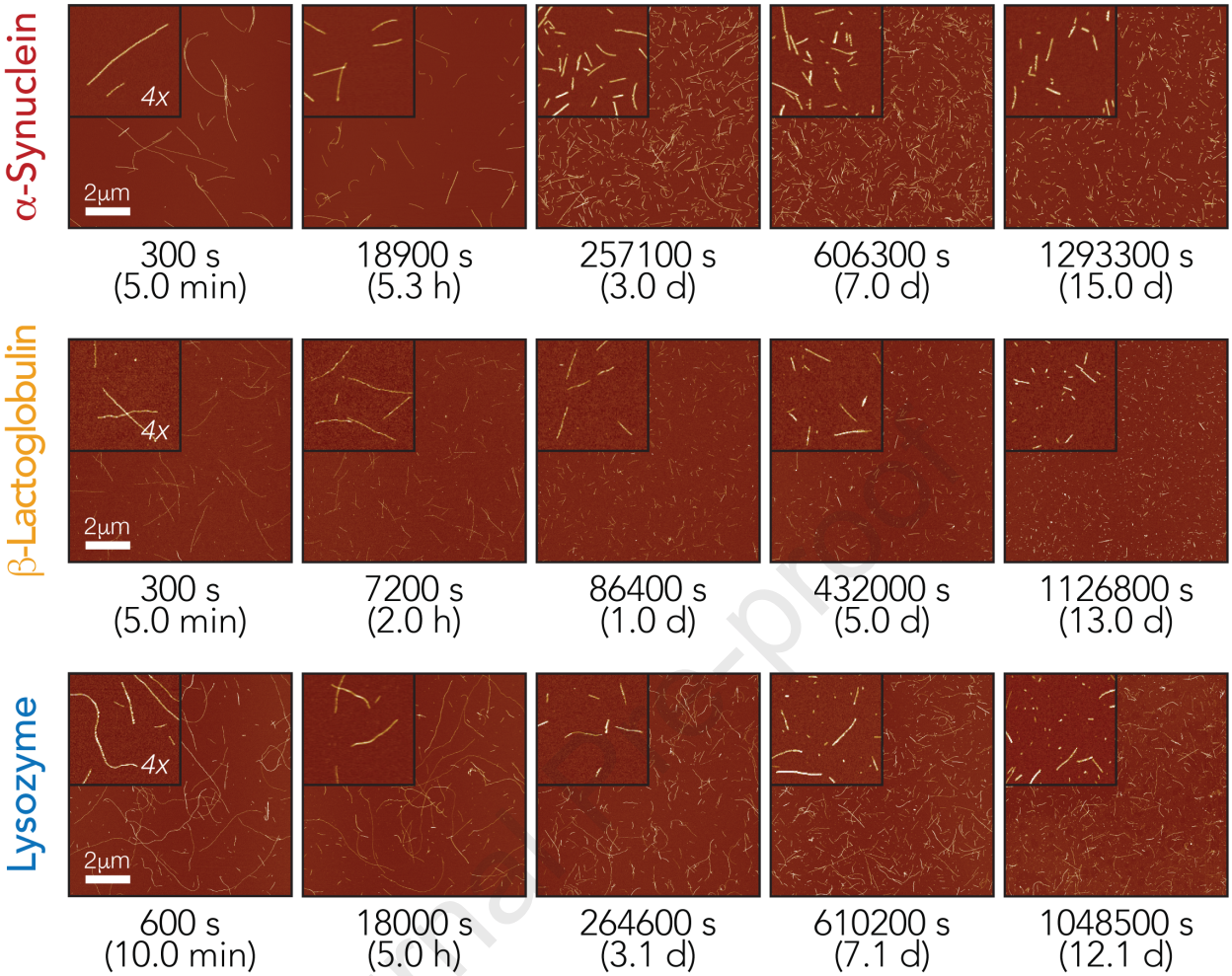

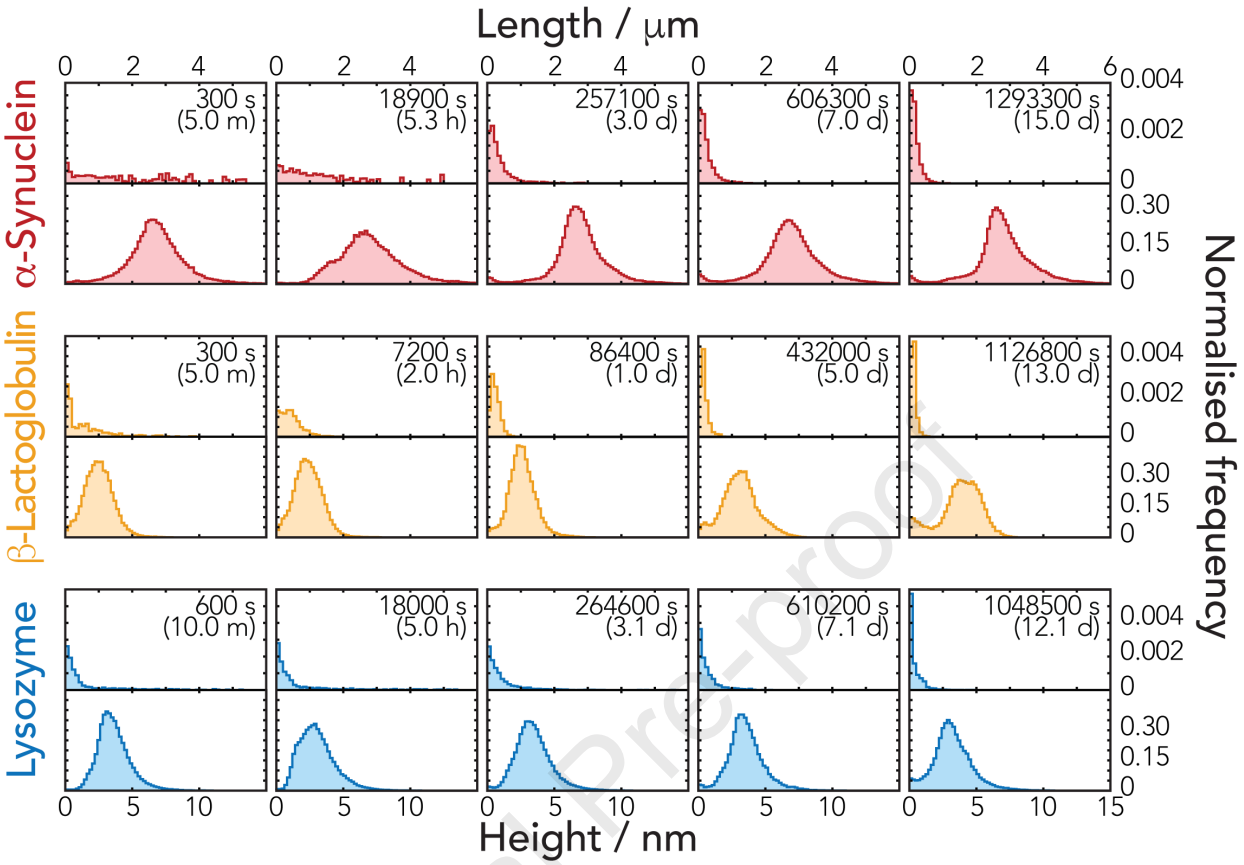

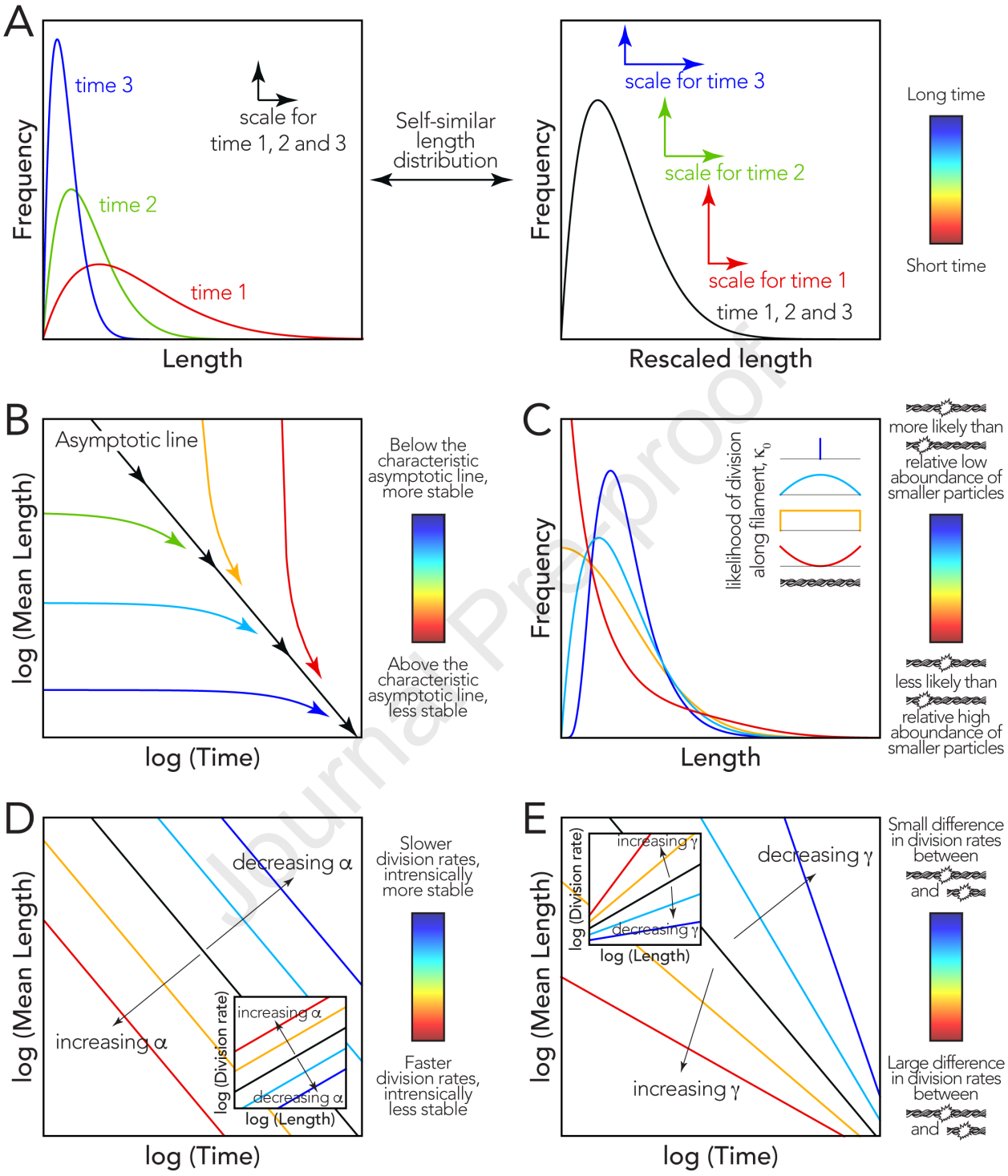
A
time 3
time 2
time 1
scale for
time 1, 2 and 3
Frequency
Length
Self-similar
length
distribution
scale for time 3
scale for time 2
scale for time 1
time 1, 2 and 3
Frequency
Rescaled length
Long time
Short time
B
Asymptotic line
log (Mean Length)
log (Time)
Below the
characteristic
asymptotic line,
more stable
Above the
characteristic
asymptotic line,
less stable
C
Frequency
Length
likelihood of division
along filament, κ_0
more likely than
relative low
abundance of
smaller particles
less likely than
relative high
abundance of
smaller particles
D
decreasing α
increasing α
log (Division rate)
increasing α
decreasing α
log (Length)
log (Mean Length)
log (Time)
Slower
division rates,
intrensically
more stable
Faster
division rates,
intrensically
less stable
E
log (Division rate)
increasing γ
decreasing γ
log (Length)
decreasing γ
increasing γ
log (Mean Length)
log (Time)
Small difference
in division rates
between
and
Large difference
in division rates
between
and

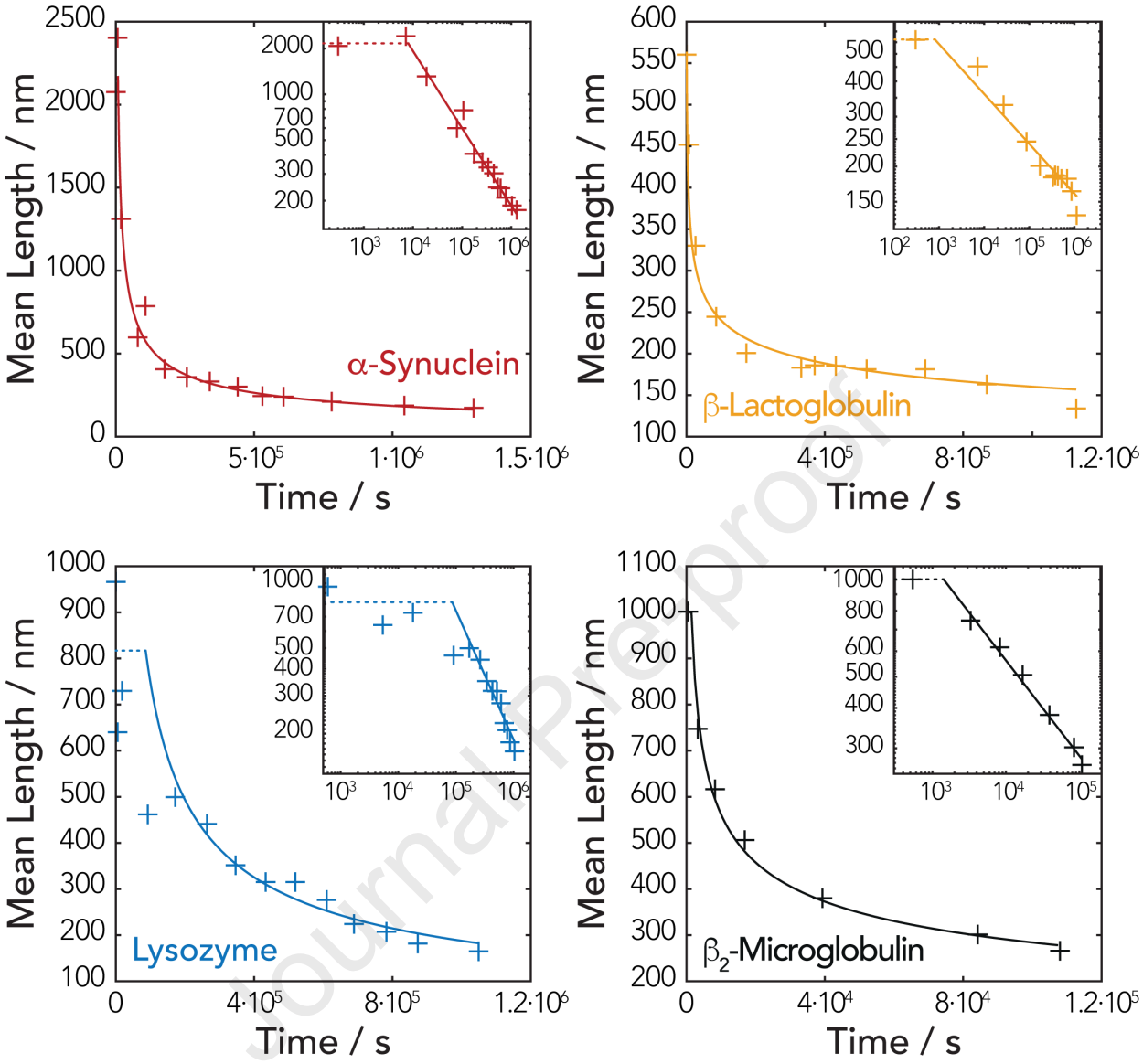

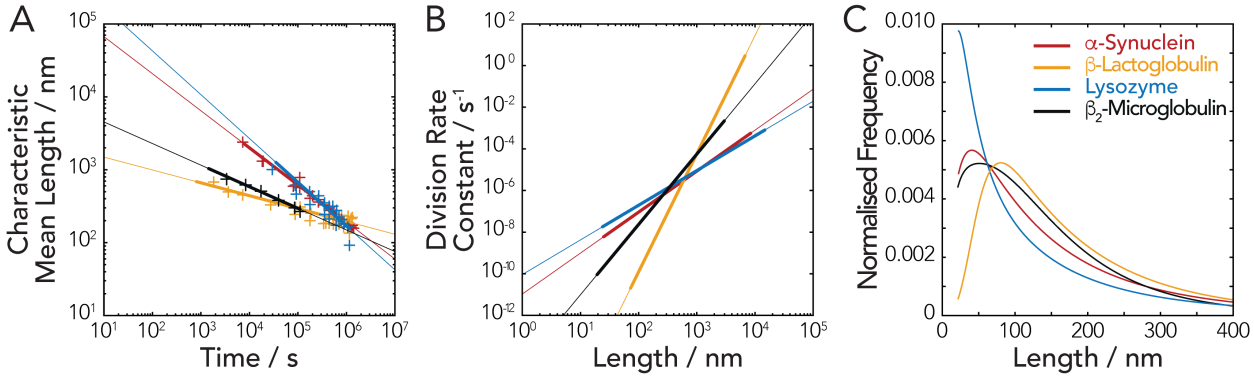

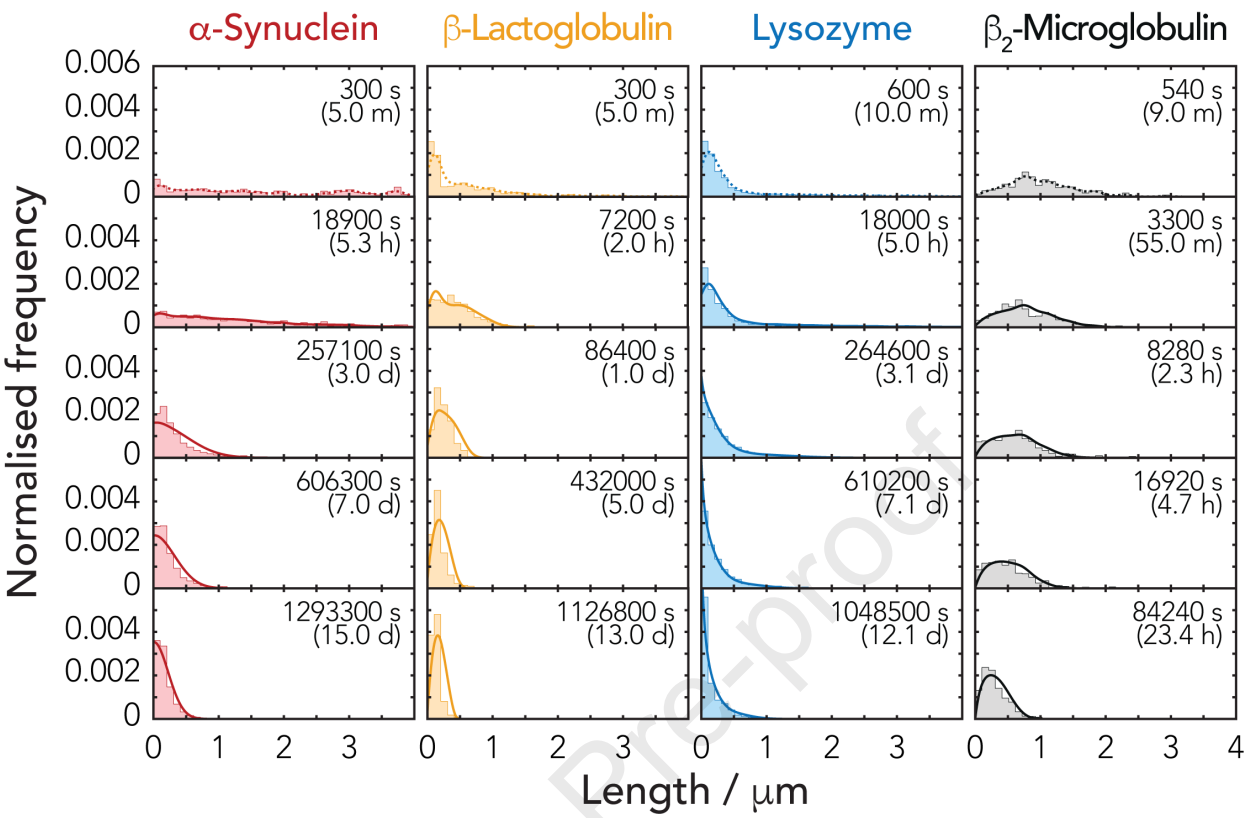

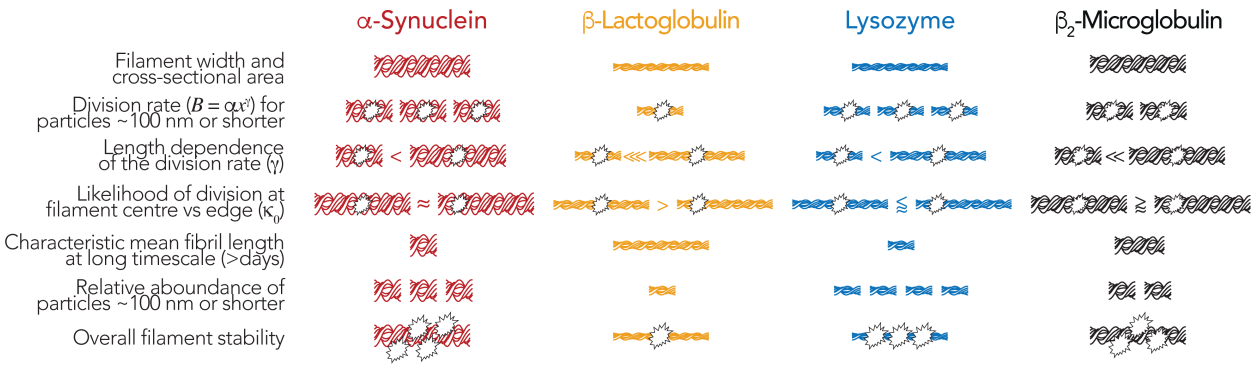

HIGHLIGHTS

- Theory on the division of amyloid fibrils developed using a continuous PDE framework
- The theory allowed direct analysis of fibril breakage properties with AFM image data
- The new insights enabled comparison of fibrils' intrinsic stability to breakage
- α-synuclein fibrils showed low stability to division compared to other model amyloid